Sequencing of RDR6-dependent double-stranded RNAs reveals novel features of plant siRNA biogenesis

Rajendran Rajeswaran, Michael Aregger, Anna S. Zvereva, Basanta K. Borah, Ekaterina G. Gubaeva and Mikhail M. Pooggin*

Institute of Botany, University of Basel, Schönbeinstrasse 6, 4056 Basel, Switzerland

ABSTRACT

Biogenesis of trans-acting siRNAs (tasiRNAs) is initiated by miRNA-directed cleavage of *TAS* gene transcripts and requires RNA-dependent RNA polymerase 6 (RDR6) and Dicer-like 4 (DCL4). Here, we show that following miR173 cleavage the entire polyadenylated parts of *Arabidopsis TAS1a/b/c* and *TAS2* transcripts are converted by RDR6 to double-stranded (ds)RNAs. Additionally, shorter dsRNAs are produced following a second cleavage directed by a *TAS1c*-derived siRNA. This tasiRNA and miR173 guide Argonaute 1 complexes to excise the segments from *TAS2* and three *TAS1* transcripts including *TAS1c* itself to be converted to dsRNAs, which restricts siRNA production to a region between the two cleavage sites. *TAS1c* is also feedback regulated by a *cis*-acting siRNA. We conclude that *TAS1c* generates a master siRNA that controls a complex network of *TAS1/TAS2* siRNA biogenesis and gene regulation. *TAS1/TAS2* short dsRNAs produced in this network are processed by DCL4 from both ends in distinct registers, which increases repertoires of tasiRNAs.

INTRODUCTION

Micro RNAs (miRNAs) regulate gene expression by silencing their target genes through mRNA cleavage and/or translational repression (1,2). In plants, some miRNA targets spawn 21-nt secondary siRNAs (3,4), a subset of which, called *trans*-acting siRNAs (tasiRNAs), can also target genes *in trans*. The tasiRNA-targeted genes can in turn spawn tasiRNAs (5), thus leading to silencing cascades which are predicted to form complex networks with distinct regulatory functions (6). miRNAs, tasiRNAs and secondary siRNAs produced from natural antisense transcripts are involved in regulation of plant development, physiology and stress responses (7–9).

The biogenesis of tasiRNAs requires RNA-dependent RNA polymerase 6 (RDR6) which converts a portion of target RNA upstream or downstream of the miRNA/siRNA cleavage site to double-stranded RNA (dsRNA). The resulting dsRNA is then processed by Dicer-like 4 (DCL4) from the miRNA-cleavage end into 21-nt in-phase siRNA duplexes with 2-nt 3′-overhangs (4,10,11).

The *Arabidopsis thaliana* genome contains four families of tasiRNA-generating *TAS* genes, classified based on miRNA-dependence, sequence similarity and target gene identity. miR173-dependent *TAS1a/b/c* and *TAS2* tasiRNAs and miR828-dependent *TAS4* tasiRNAs are encoded downstream of the miRNA cleavage site and target the genes of pentatricopeptide repeat and MYB transcription factor families, respectively (3,4). miR390-dependent *TAS3a/b/c* tasiRNAs are encoded upstream of the miRNA-cleavage site and target the genes of auxin response factor family (4,10).

One of the open questions concerning secondary siRNA biogenesis is which factors route some (but not all) miRNA/tasiRNA target transcripts into the RDR6/DCL4 pathway. For the *Arabidopsis TAS3* family, a second, non-cleavable, miR390-binding site located upstream of the miR390 cleavage site is essential for tasiRNA biogenesis (12) and the region of *TAS3a/b/c* transcripts between the two miR390 sites spawns most of secondary siRNAs including tasiRNA species (4). Interestingly, *TAS3* transcripts from moss and pine are cleaved at both miR390-target sites (12). These results, together with a finding that secondary siRNAs more often emanate from the genes with two known miRNA/tasiRNA target sites, suggested a two-hit trigger model for secondary siRNA biogenesis (12,13). However, this model

left unexplained a robust production of siRNAs from miR173-dependent *TAS* genes. Efforts to identify a second hit by a known small RNA or some other transcript feature required for tasiRNA production have failed so far (14).

miRNAs and siRNAs exert their silencing functions in association with Argonaute (AGO) proteins that sort sRNAs based on size and 5′-terminal nucleotide (13,15,16). Thus, AGO1 binds mostly 21-nt RNAs with 5′-terminal uridine (5′U), while AGO2 binds mostly 21-nt RNAs with 5′-terminal adenine (5′A). Interestingly, both miR173 and miR390 that initiate tasiRNA biogenesis deviate from this general rule. miR390 is a 21-nt 5′A-RNA but it is specifically associated with AGO7 that plays an essential role at both cleavable and non-cleavable *TAS3* target sites (13,17). miR173 is a 22-nt 5′U-RNA that associates with AGO1 to guide the cleavage of *TAS1a/b/c* and *TAS2* transcripts (14). The 22-nt size of miRNA is sufficient to trigger RDR6-dependent siRNA production from miRNA target transcripts including miR173 targets (18,19). A more recent study, however, indicates that asymmetrically positioned bulged bases in a miRNA:miRNA* duplex are more important than the miRNA length for the initiation of RDR6-dependent siRNA biogenesis (20).

Here we used blot hybridization and circularization-reverse transcription-PCR (cRT-PCR) to characterize the structures of dsRNAs originating from *Arabidopsis* miR173-dependent *TAS* genes and immunoprecipitation (IP) to identify tasiRNAs associated with AGO complexes. Our study uncovers a complex sRNA network connecting *TAS2* and *TAS1* genes which is controlled by miR173 and a *TAS1c*-derived tasiRNA.

MATERIALS AND METHODS

Arabidopsis wild-type, *rdr6-15 and dcl* mutant lines used in this study, their growth conditions and infection with CaMV, and the detailed protocols for total RNA preparation and high-resolution blot hybridization have been described earlier (21,22). *ago1-25* and *ago2-1* were kindly provided by Dr Baulcombe. Seeds of *tas1c-1* (SAIL_242_C04) were obtained from the Arabidopsis Biological Resource Center and the homozygous individuals were identified by genotyping. Probes used for RNA blot hybridization and genotyping are listed in Experimental Procedures in Supplementary Data. cRT-PCR mapping of *TAS* RNAs was performed as described earlier [(23); for details, see Methods in Supplementary Data].

The IP experiment with native AGO1-antibodies (Agrisera) and blot hybridization analysis of AGO1-associated sRNAs were performed as we described recently (24). The sRNA probes are listed in Methods in Supplementary Data.

Transient expression experiments using *Nicotiana benthamiana* were performed as described previously (10). The 35S:TAS1c construct was mutagenized by replacing the region between *Pfo I* and *Pac I* sites with synthetic gene fragments carrying the corresponding

mutations. For further details, see Methods in Supplementary Data.

RESULTS

Long and short co-terminal dsRNAs originate from all miR173-targeted *TAS* genes

Previously we found that infection with *Cauliflower mosaic virus* (CaMV) leads to stabilization of RDR6-dependent precursors of tasiRNAs in *Arabidopsis* (21). Using high-resolution gel separation of total RNA followed by blot hybridization with DNA oligonucleotide probes specific for *TAS1* and *TAS2* loci, we further characterized the stabilized sense (S) and antisense (AS) precursors (Figure 1). To investigate DCL requirements for dsRNA biogenesis, we compared CaMV-infected wild-type *Arabidopsis* (Col-0 and La-er) with double (*dcl2/3* and *dcl3/4*) and triple (*dcl2/3/4*) *DCL*-mutant lines [all in Col-0 background; (22)]. All the mutants still express DCL1 that produces miRNAs.

Given that tasiRNA siR255 is encoded in sense strands of all three *TAS1* genes (*1a*, *1b* and *1c*) the probe complementary to siR255 would detect their primary Pol II transcripts (pri-RNAs) and the sense strands of RDR6-dependent dsRNAs. The probe complementary to the star strand of siR255/siR255* duplex would detect only the antisense strand of RDR6-dependent dsRNAs. The two probes gave identical hybridization patterns in the range of 100–600 nt (Figure 1A), indicating that the RNAs detected within this range can potentially be sense and antisense strands of distinct dsRNA precursors of siR255/siR255*. To further classify these RNAs, we used the probes specific to the 21-nt sequences adjacent to the miR173 cleavage site (identical in both *TAS1a* and *TAS1b* but not *TAS1c*) and the probe specific to *TAS1b* (Figure 1A). The resulting hybridization patterns allowed to identify the pri-RNAs and putative dsRNAs produced from each of the three *TAS1* loci (Figure 1B). Likewise, probes specific for the *TAS2* sequences identified one major and several minor sense/antisense RNA pairs (Figure 1).

Comparison of the hybridization patterns in wild-type versus *dcl*-mutant lines indicated that most of the *TAS1* and *TAS2* putative dsRNAs, except for the longest species, require DCL4 activity for their biogenesis. The longest sense/antisense pair derived from each locus over-accumulated in *dcl2/3/4* (Figure 1A). The longest and shorter pairs from each locus, except for one *TAS1b* and two *TAS2* non-abundant pairs (Figure 1B; designated DCL4 processing intermediates), all contain sequences adjacent to the miR173 cleavage site. Thus, most of the shorter dsRNAs are not intermediates of DCL4 processing of the longest dsRNAs from the miR173 end. The results described below are consistent with this conclusion.

Confirming our previous results (22), CaMV-infected *rdr6-15* mutant plants, which lack RDR6 activity, did not accumulate any *TAS1/TAS2*-derived sense/antisense RNA pairs. Only sense strands of the longest dsRNAs, i.e. miR173-cleavage products of *TAS1/TAS2* pri-RNAs
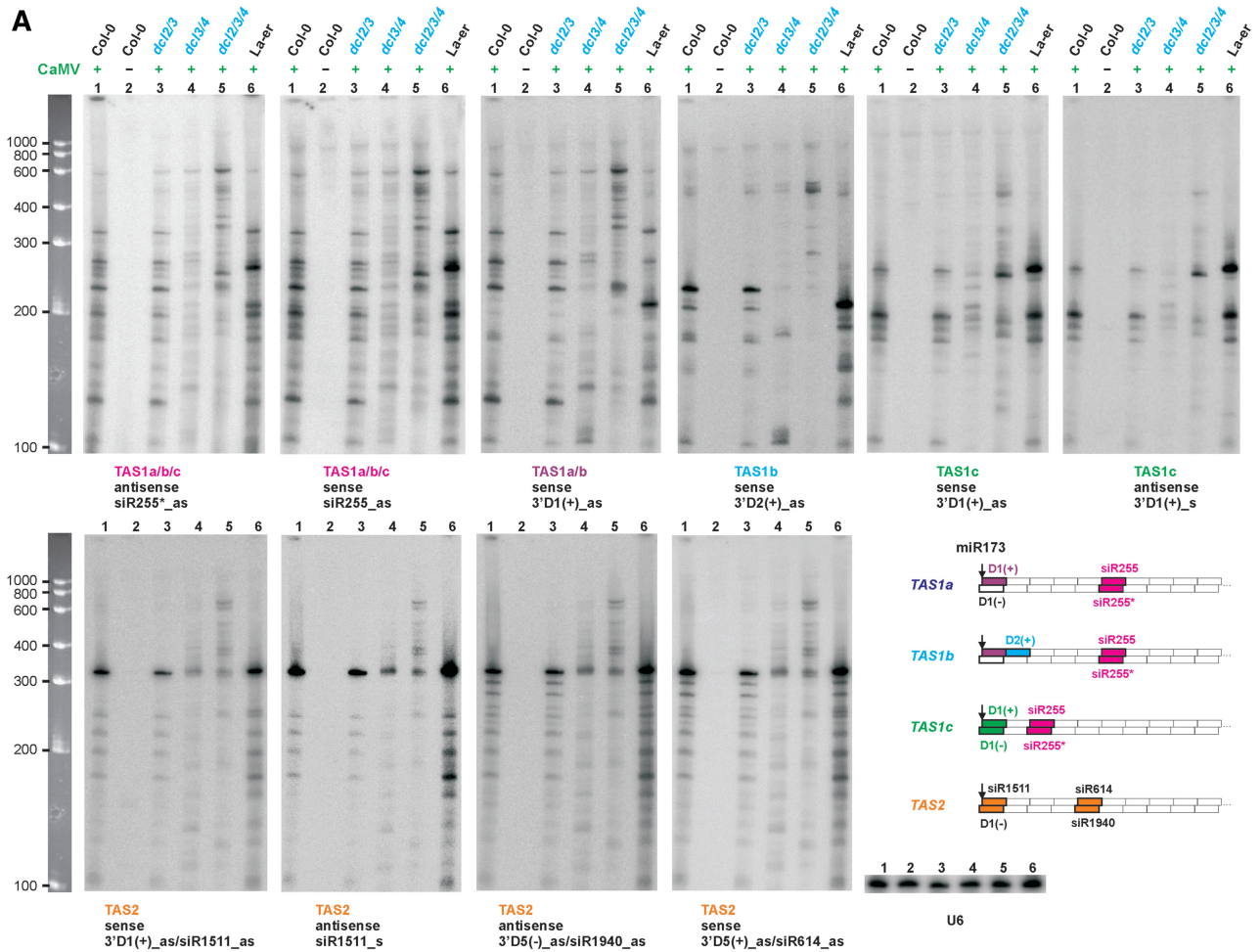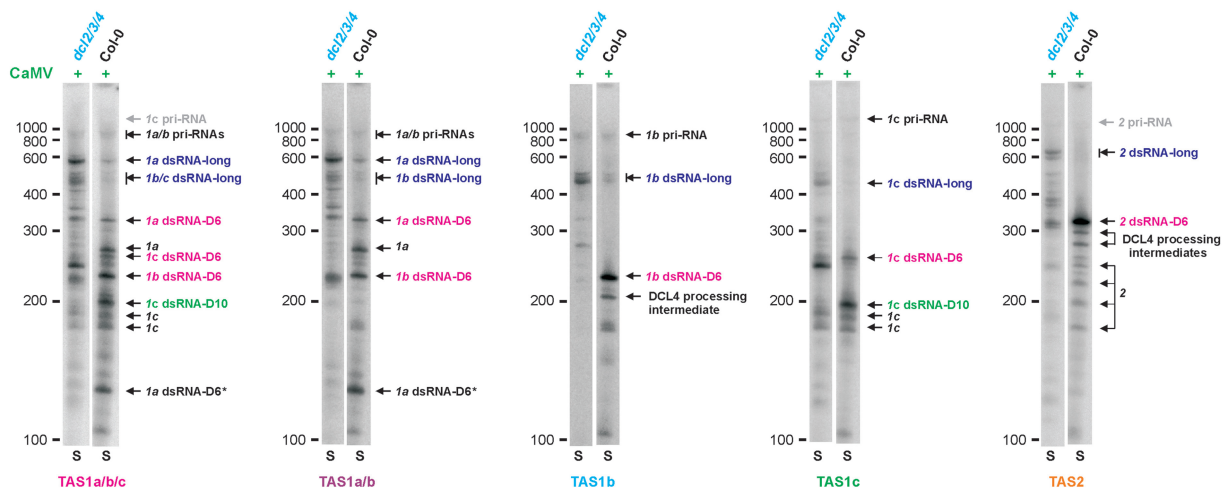
Figure 1. Blot hybridization analysis of dsRNA precursors of *TAS1a/b/c* and *TAS2* tasiRNAs. (**A**) The panel shows blot hybridization analysis (5% PAGE) of total RNA from CaMV-infected (+) or mock-inoculated (−) wild-type (Col-0 and La-er), double (*dcl2/3* and *dcl3/4*) and triple (*dcl2/3/4*) DCL-deficient mutants. The scans represent the same blot successively hybridized with probes specific for *TAS1a/b/c-*, *TAS1a/b-*, *TAS1b-*, *TAS1c-* and *TAS2*-derived 21-nt siRNAs and U6 RNA as a loading control. Single-stranded RNA markers are shown on the left. The scheme shows location and polarity of the probed siRNAs (colored boxes with their names indicated) with respect to the miR173 cleavage site (indicated by arrow) on hypothetical dsRNAs from the four *TAS* genes. Identical siRNAs/probes, i.e. siR255/siR255* duplex encoded by *TAS 1a*, *1b* and *1c* and 3′D1(−) siRNA of *TAS 1a* and *1b*, are indicated in pink and purple, respectively. Cyan, blue and orange indicate siRNAs/probes specific for *TAS1b*, *TAS1c* and *TAS2*, respectively. (**B**) Interpretation of the analysis shown in panel A. The lanes corresponding to Col-0 and *dcl2/3/4* samples were cropped from the above blots of sense (S) polarity. Positions of pri-RNAs and dsRNAs are indicated by arrows for each *TAS* gene (*1a*, *1b*, *1c* and *2*).

(see below), could be detected by blot hybridization in *rdr6-15* (Supplementary Figure S1).

Polyadenylated 3′-products of miR173-cleaved *TAS* pri-RNAs are entirely converted by RDR6 to dsRNAs

To precisely map *TAS* dsRNAs we used cRT-PCR that allows simultaneous sequencing of 5′- and 3′-termini of a given RNA [(23), Supplementary Figure S2A]. Pyrophosphatase treatment of total RNA, prior to RNA ligation, allowed circularization of transcripts not only with a 5′-monophosphate present on 3′-fragments of miRNA-cleaved *TAS* pri-RNA, but also with a 5′-triphosphate likely present on an RDR6-synthesized complementary RNA. cRT-PCR primers proximal to the termini of a given sense or antisense RNA (Figures 2 and 3; Supplementary Figure S2) were designed based on the sizes of putative dsRNAs estimated by blot hybridization (Figure 1B). cRT-PCR products were gel-purified, cloned and sequenced (∼10–30 individual clones for each).

For each *TAS*, we first mapped the longest sense/antisense RNA pair from wild-type (Col-0) and *dcl2/3/4* plants. Typically, no abundant products could be obtained using total RNA from mock-inoculated *Arabidopsis*, whereas the CaMV-infected material-yielded abundant cRT-PCR products of expected size (Supplementary Figure S2). Along with our blot hybridization (Figure 1), this indicates that tasiRNA precursors are efficiently processed by DCLs and do not accumulate at high levels, unless they are stabilized [in our case by the CaMV transactivator protein; (21)]. cRT-PCR analysis revealed that most of the *TAS1a* longest sense RNAs are the entire 3′-products of miR173-directed cleavage of the pri-RNA: they start with U379 (numbered from the cap site) and terminate with a poly(A) tail of up to 24 nt attached at one major site (A933) and several minor sites (Figure 2 and Supplementary Figure S2A). One to three terminal uridines were attached to some poly(A) tails. Most of the *TAS1a* longest antisense RNAs (RDR6 products) terminate with A379 and a large fraction of those start with a poly(U) stretch of up to 26 nt attached to U933 or at nearby positions. Some antisense RNAs have short A-rich stretches at the very 5′-end (Supplementary Figure S2A). Thus, the antisense RNAs are essentially complements of the sense RNAs. These results demonstrate that RDR6 copies the entire 3′-product of miR173-cleaved *TAS1a* pri-RNA into a complementary RNA.

cRT-PCR analysis of the longest dsRNAs from *TAS1b*, *TAS1c* and *TAS2* genes (Supplementary Figure S2B, S2C and S2D, respectively) led us to similar conclusions with some peculiarities in each case. For *TAS1b*, two major (U753 and A822) and several minor poly(A) sites were identified (Figure 2 and Supplementary Figure S2B). The longest antisense RNAs from *TAS1b* have very short U-stretches, UA-rich stretches or just a single uridine at the 5′ termini, suggesting that long poly(A) tails are almost entirely removed from the 3′-cleavage product before its conversion to dsRNAs. For *TAS1c*, two major poly(A) sites were mapped (A810 and G816), one of which (A810) was reported earlier (14). *TAS1c* pri-RNAs of both types are used as templates for RDR6 following miR173-cleavage, since the counterpart antisense RNAs with long U-stretches at the 5′-end were found (Figure 2 and Supplementary Figure S2C). The longest *TAS2* dsRNAs were composed of miR173-cleaved pri-RNA terminating at several minor and one major (A1031) poly(A) sites and their antisense counterparts (Figure 2 and Supplementary Figure S2D). Notably, in this case the longest dsRNAs could be detected by cRT-PCR only in *dcl2/3/4* but not in wild-type plants, which is consistent with the blot hybridization analysis (Figure 1).

A second cleavage of miR173-targeted *TAS* pri-RNAs generates an additional template for RDR6

cRT-PCR results summarized in Figure 3 show that sense RNA of the most abundant sense/antisense pair derived from *TAS2* in wild-type plants starts with U418 and ends predominantly with G734. Thus, this RNA is a derivative of the miR173-cleaved pri-RNA 3′-product truncated by a second, downstream cleavage. The corresponding antisense RNA starts with A732 and ends with A418 (Figure 3). Thus, RDR6 synthesis of a complementary RNA begins at the third nucleotide of the sense template, which creates a 2-nt 3′-overhang at the end of the resulting dsRNA, and stops at the template's last nucleotide. A large fraction of the antisense RNAs contained one to three non-template nucleotides, predominantly UU or UA (Supplementary Figure S2D). Since a tomato RDR activity was reported to add one non-template nucleotide to a fraction of the run-off antisense transcripts *in vitro* (25), we assume that the *Arabidopsis* RDR6 has a similar property *in vivo*. cRT-PCR analysis of the shorter *TAS2* dsRNAs in *dcl2/3/4* plants which lack DCL4 activity revealed heterogeneous populations of sense and antisense RNAs with the sense RNAs starting at the miR173 cleavage site but ending at various positions and the antisense RNAs mirroring their sense counterparts (Supplementary Figure S2D). We conclude that *TAS2* pri-RNA is cleaved twice, first at the miR173 site and second at the downstream site by a cleavage indirectly dependent on DCL4. The 317-nt RNA fragment between the two cleavage sites is converted by RDR6 to a 315-bp dsRNA (Figure 1). This dsRNA has a 2-nt 3′-overhang at the second cleavage end and an up to 3-nt 3′-overhang at the miR173 end.

cRT-PCR analysis of *TAS1b* short sense RNA also revealed a second, DCL4-dependent, cleavage site downstream of the miR173 site: all the cloned RNAs start with A374 and end with G601 (Figure 3 and Supplementary Figure S2B). The corresponding antisense RNA starts either with C600 or U599 and ends predominantly with U374 followed in 50% cases by one or two non-template uridines (Supplementary Figure S2B). Thus, the most abundant precursor of *TAS1b* tasiRNAs is 227- or 226-bp dsRNA with a 2-nt 3′-overhang at the second cleavage end and an up to 2-nt 3′-overhang at the miR173 end.
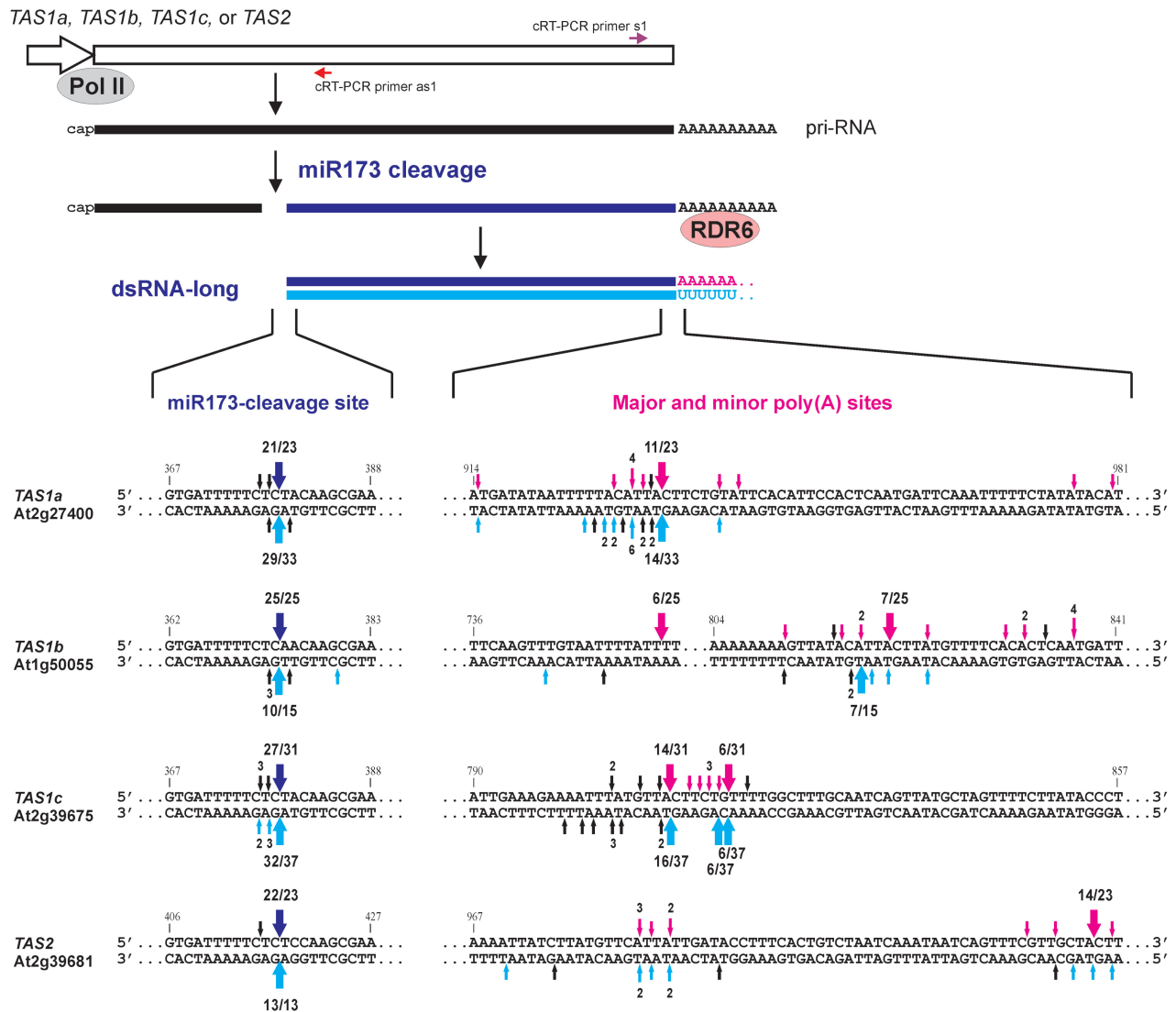
Figure 2. The entire, polyadenylated 3′-products of miR173-cleaved pri-RNAs of *TAS1a*, *TAS1b*, *TAS1c* and *TAS2* genes are converted by RDR6 to dsRNAs. Diagrammatic representation of *TAS* genes transcribed by Pol II into 5′-capped and 3′-polyadenylated pri-RNAs which are then cleaved by miR173-AGO1 complexes. The 3′-products are converted by RDR6 to long dsRNAs. The regions of the miR173 cleavage site and the poly(A) sites of each *TAS* pri-RNA are enlarged. Arrows above the upper strand indicate positions of the 5′-terminus (miR173 site) and the 3′-terminus of at least one cloned cRT-PCR product representing the sense strands of *TAS* dsRNAs; the 3′-termini to which poly(A) is added are indicated in pink. Arrows below the complementary strand indicate the termini of one or more cloned cRT-PCR product representing the corresponding antisense strands of dsRNAs. Termini of the antisense RNA that begin with a poly(U) stretch are indicated in cyan. Thick arrows indicate the termini of the major sense and antisense RNAs; the number of specific cRT-PCR products/total products sequenced for each strand are indicated. Positions of cRT-PCR primers used for long dsRNA mapping are indicated above and below of the *TAS* gene body.

The *TAS1a* sense/antisense pair of ∼320 bp is more abundant than the *TAS1a* longest dsRNA but less abundant than two shorter pairs derived from this locus (Figure 1B). cRT-PCR mapping showed that this dsRNA is produced by the two-cleavage mechanism involving miR173-directed and DCL4-dependent cleavages. These cleavages excise a 318-nt fragment from *TAS1a* pri-RNA (from U379 to U696) which is copied by RDR6 to the complementary RNA starting either with U694 or C695 and ending with A379, often followed by one or two non-template nucleotides (Figure 3 and Supplementary Figure S2A). Thus, this dsRNA resembles the most-abundant *TAS1b* dsRNA.

TAS1c-derived tasiRNA directs a second cleavage of *TAS2*, *TAS1a* and *TAS1b* pri-RNAs

Our inspection of the second cleavage sites mapped on *TAS2*, *TAS1b* and *TAS1a* pri-RNAs revealed a remarkable similarity: all these sites are near-perfectly complementary to the *TAS1c*-derived siRNA 3′D6(−); this siRNA is encoded at the sixth processing cycle from the miR173-cleavage site in the antisense orientation (4,10). In all three cases, the cleavage occurs within a target pri-RNA/tasiRNA duplex between positions 10 and 11 from the tasiRNA 5′-end (Figure 3), thus representing a conserved, AGO-mediated cleavage. Inspection of sRNA deep-sequencing data [http://asrp.cgrb.oregonstate.edu;
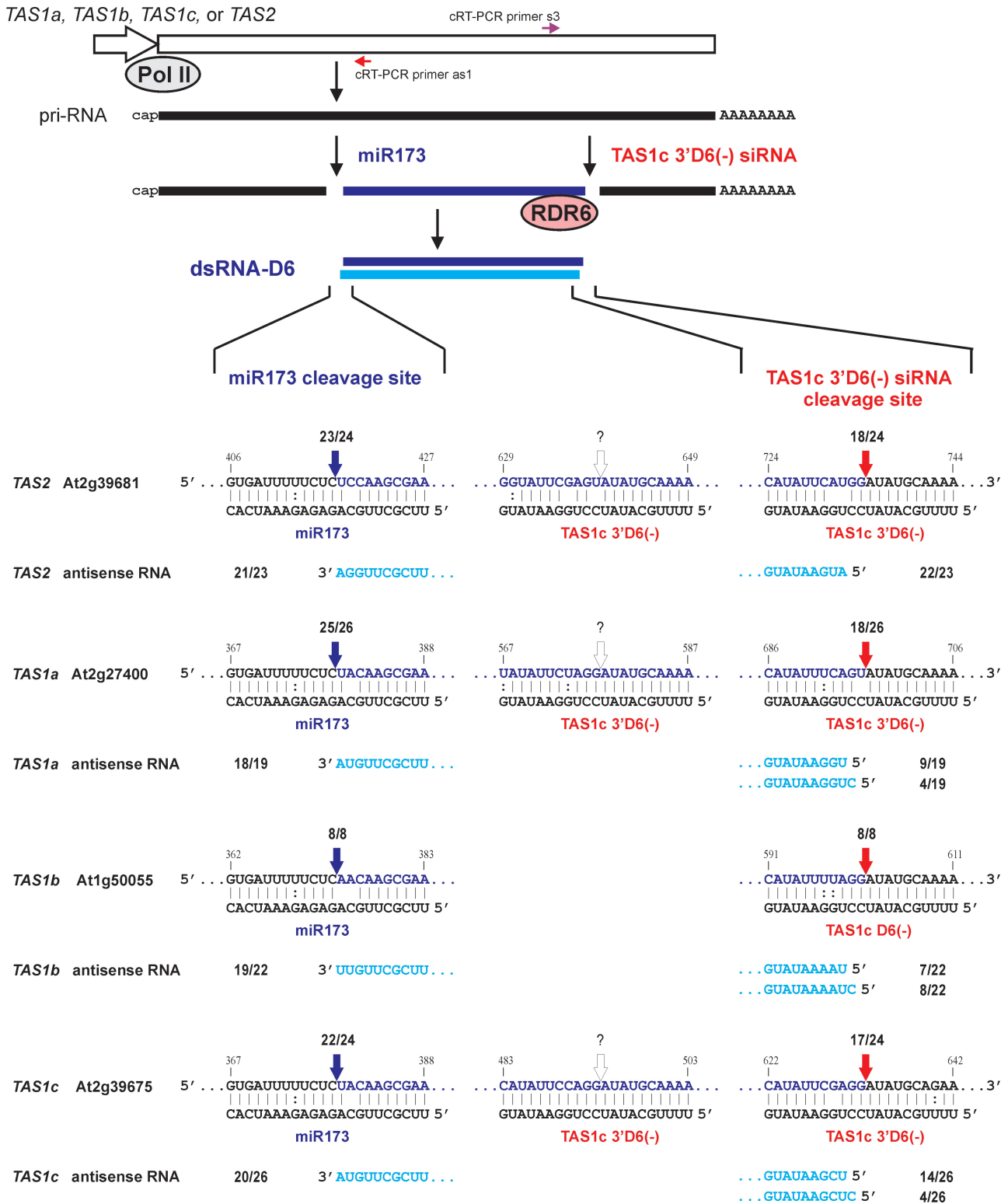
Figure 3. Two-cleavage mechanism for biogenesis of *TAS1a*-, *TAS1b*-, *TAS1c*- and *TAS2*-derived dsRNAs. Diagrammatic representation of *TAS* genes transcribed by Pol II into pri-RNAs which are then cleaved at the two sites by miR173- and *TAS1c* 3′D6(−) siRNA-AGO1 complexes, respectively. The excised fragment between the two-cleavage sites is converted by RDR6 to dsRNA. The cleavage sites for each pri-RNA and the siRNA/target pri-RNA duplexes are shown in the expanded regions. Additional complementary sites for *TAS1c* 3′D6(−) siRNA in the intervening regions of *TAS2* and *TAS1a* pri-RNAs as well as the origin site of *TAS1c* 3′D6(−) are also shown. Colored arrowheads indicate positions of the 5′-terminus (miR173 site; in blue) and the 3′-terminus [*TAS1c* 3′D6(−) site; in red] of cloned cRT-PCR products representing the sense strands of *TAS* dsRNAs. The 5′- and 3′-terminal sequences of cRT-PCR clones representing the corresponding antisense strands of TAS dsRNAs are shown below the duplexes and highlighted in cyan. The number of specific cRT-PCR products/total products sequenced for each strand is indicated. Positions of potential cleavage sites for 3′D6(−) siRNA are indicated by open arrowheads. Positions of the cRT-PCR primers used for the short dsRNA mapping are indicated above and below of the *TAS* gene body.
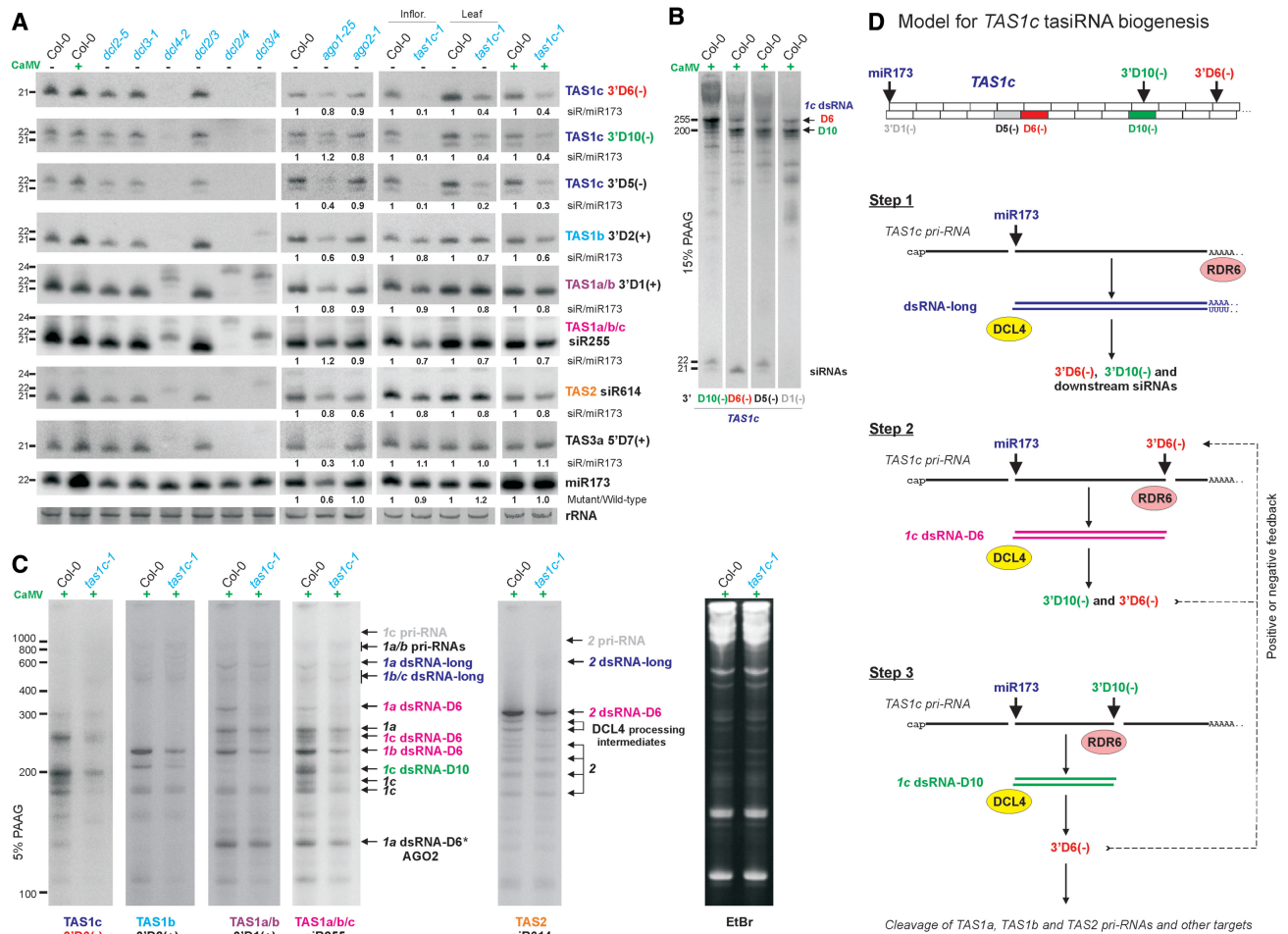
Figure 4. *TAS1c* is a master tasiRNA-generating unit regulated by feedback loops. (**A**) Genetic requirements for the biogenesis of *TAS1/2*-derived siRNAs. The panel shows blot hybridization analysis (15% PAGE) of total RNA from CaMV-infected (+) or mock-inoculated (−) wild-type *Arabidopsis* (Col-0), single (*dcl2-5*, *dcl3-1* and *dcl4-2*) and double (*dcl2/3*, *dcl2/4* and *dcl3/4*) DCL null mutants, AGO mutants (*ago1-25* and *ago2-1*) and *TAS1c* siRNA-deficient mutant (*tas1c-1*) plants. The cropped scans represent blots successively hybridized with probes specific for *TAS1c-*, *TAS1b-*, *TAS1a/b-*, *TAS1a/b/c-*, *TAS2-* and *TAS3a*-derived siRNAs and miR173. EtBr-stained rRNA is shown as a loading control. The relative levels of *TAS* siRNA accumulation in a mutant line versus Col-0 were calculated using the miR173 level as an internal control for each sample; for each blot, siRNA levels in Col-0 were set to 1. (**B**) Blot hybridization analysis of *TAS1c*-derived dsRNA-D6 and dsRNA-D10. The cropped scans are from the blot shown in panel (A) (the second lane from left). (**C**) Blot hybridization analysis of *TAS1c-*, *TAS1b-*, *TAS1a-*, *TAS2-*derived dsRNAs in CaMV-infected Col-0 and *tas1c-1* plants using 5% PAGE. The total RNA samples analyzed are the same as in panel A (the two from right). EtBr-stained RNA is shown as a loading control. Positions of dsRNAs derived from *TAS1c*, *TAS1b*, *TAS1a* and *TAS2* are indicated by arrows (same as in Figure 1B). *TAS1c* 3′D6(−) tasiRNA-dependent dsRNAs are highlighted in pink, *TAS1c* 3′D10(−)-dependent dsRNA is in green and tasiRNA-independent longest dsRNAs are in blue. (**D**) Model for *TAS1c* tasiRNA biogenesis and feedback regulation.

(4)] showed that this 21-nt RNA is one of the most abundant siRNAs derived from *TAS1c*. It is shifted forward by 1 nt with respect to the 21-nt phase set by miR173 cleavage, because a 22-nt siRNA/siRNA* duplex is generated at the fourth or the fifth processing cycle (Supplementary Figure S3A). The 1-nt phase forward drift was also found to occur in *TAS3a* and may result from misprocessing by DCL4 (4).

Consistent with the deep-sequencing data, our blot hybridization showed that *TAS1c* 3′D6(−) appears as one 21-nt class, while 3′D5(−) accumulates as minor (21 nt) and major (22 nt) classes (Figure 4A). Genetic analysis revealed that the biogenesis of both 3′D6(−) and 3′D5(−) requires DCL4, with no substantial contribution of DCL2, the dicer normally involved in generating 22-nt RNAs (Figure 4A).

The 3′D6(−) is a 21-nt 5′U-RNA which would predict its association with AGO1 (15). Indeed, our IP experiment using native AGO1-antibodies revealed that AGO1 protein binds this siRNA as tightly as miR173 (Figure 5A). We conclude that both miR173 (18) and *TAS1c* 3′D6(−) tasiRNA guide AGO1-mediated cleavage of *TAS2* and *TAS1a/b* pri-RNAs at their respective target sites.

We also identified additional target sites for *TAS1c* 3′D6(−) on *TAS2* and *TAS1a* pri-RNAs, each located between the two mapped cleavage sites (Figure 3).

TAS1c 3′D6(−) directs *in trans* cleavage of *TAS1c* pri-RNA downstream of the origin site, which leads to its shorter dsRNA precursor

TAS1c 3′D6(−) has the potential to cleave its own precursor (*TAS1c* pri-RNA) *in cis*, i.e. at the site of its origin
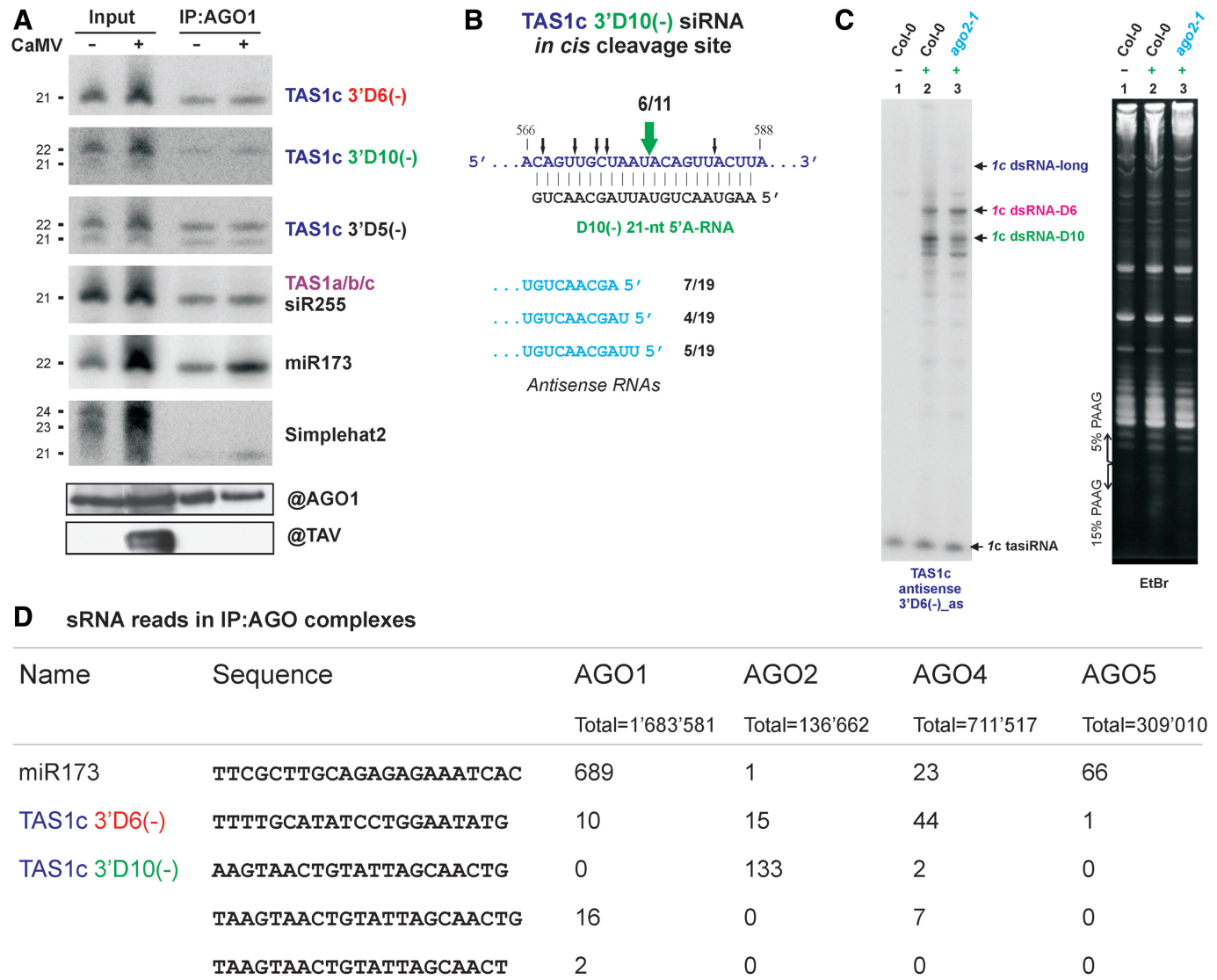
Figure 5. Loading of TAS1c siRNAs into AGO1 and AGO2 complexes that mediate *in trans* and *in cis* cleavages. (**A**) The upper panel shows blot hybridization analysis of total sRNAs (input) and sRNAs associated with AGO1 protein in mock-inoculated (−) or CaMV-infected (+) plants following IP with AGO1-antibodies (IP:AGO1). The scans represent the same blot successively hybridized with probes specific for *TAS1c* siRNAs, miR173 and, as a negative control, the transposon *SIMPLEHAT2*-derived 24-nt siRNA. The lower panel shows Western blot analysis of AGO1 protein accumulation in the input and the IP:AGO1 fractions using AGO1-antibody (@AGO1). Underneath is the same blot stained with antibodies specific for CaMV TAV protein (@TAV); (**B**) The *in cis* cleavage site for *TAS1c*-derived siRNA 3′D10(−) at *TAS1c* pri-RNA (the numbering is from the 5′ cap-site). Thick and thin arrows indicate the major and minor cleavage products, respectively, determined by cRT-PCR; the number of clones is given when more than one clone had the same 3′-terminus. The sequence of 3′D10(−) siRNA guiding the cleavage is shown under the pri-RNA sequence. The 5′-termini of predominant antisense RNAs of *1c* dsRNA-D10 are shown, with corresponding numbers of specific cRT-PCR products/total products indicated; (**C**) Blot hybridization analysis of *TAS1c*-derived dsRNAs in CaMV-infected Col-0 and *ago2-1* plants using 5% PAGE. The blot was hybridized with TAS1c 3′D6(−) siRNA-specific probe. EtBr-stained RNA is shown as a loading control. Positions of *TAS1c*-derived dsRNAs and dsRNA-D10 are indicated by arrows; (**D**) sRNA sequencing reads for *TAS1c*-derived siRNAs and miR173 in sRNA libraries prepared from AGO:IP complexes [(15); GEO accession: GSE10036].

(Figure 3), which together with miR173-cleavage would give rise to a 115-nt fragment. However, we did not detect any abundant sense or antisense RNA of this size with *TAS1c* probes (Figures 1 and 4B). Instead, we identified another complementary site for *TAS1c* 3′D6(−) in a downstream position of *TAS1c* pri-RNA, and confirmed by cRT-PCR that it is cleaved at the expected position (Figure 3 and Supplementary Figure S2C). The 255-nt fragment (U378 to G632) excised from *TAS1c* pri-RNA by miR173 and TAS1c 3′D6(−) is converted to

dsRNA with 1 or 2-nt 3′-overhangs on both ends, since the termini of the corresponding antisense RNA were mapped to positions C631 or U630 (5′ end) and A378 (3′-end); two non-template nucleotides were added in most cases (Figure 3 and Supplementary Figure S2C). A sense/antisense RNA pair of the corresponding size is the second most abundant *TAS1c* pair detected by blot hybridization (Figures 1 and 4B; Supplementary Figure S2C; designated *1c* dsRNA-D6). This finding is indicative of a feedback loop regulating *TAS1c* 3′D6(−) biogenesis (Figure 4D).

The most abundant precursor of *TAS1* 3′D6(−) is generated via *in cis* cleavage

The most abundant sense/antisense RNA pair derived from *TAS1c* is shorter than the earlier described *1c* dsRNA-D6 (Figures 1 and 4B; designated *1c* dsRNA-D10). cRT-PCR (Supplementary Figure S2C) revealed that it is generated by a two-cleavage mechanism involving miR173 and *TAS1c*-derived siRNA 3′D10(−) which appears to cleave *TAS1c* pri-RNA *in cis* at the sites of its origin (Figure 5B). The sense strand of the resulting dsRNA starts with U379 and terminates predominantly with U577. The antisense strand 5′-ends map predominantly to U576, U575 and A574, thus resulting in 1- to 3-nt 3′-overhang (Figure 5B). The corresponding 3′-ends map to A379 followed with a few non-template nucleotides (Supplementary Figure S2C).

The 3′D10(−) itself can be generated from both *TAS1c* longest dsRNA and *1c* dsRNA-D6 (Figure 4C) by DCL4 processing at the tenth cycle from the miR173 end. On blots, the 3′D10(−) appears as 21-nt and, more abundant, 22-nt classes (Figure 4A). The mapped cleavage site on *TAS1c* pri-RNA would predict that both size-classes should have 5′-terminal A587 to direct an AGO-mediated cleavage at the mapped position (Figure 5B).

Genetic analysis showed that both 21-nt and 22-nt classes of *TAS1c* 3′D10(−) require DCL4 for their biogenesis. The 21-nt class is selectively reduced in the null mutant *ago2-1* (15), whereas the 22-nt class is selectively reduced in the hypomorphic mutant *ago1-25* (26) (Figure 4A). This suggests that *TAS1c* 3′D10(−) exists as 21-nt 5′A587-RNA bound to AGO2 and 22-nt 5′U588-RNA bound to AGO1. Our AGO1-IP and other AGO-IP studies support this conclusion (Figure 5A and D).

Taken together, our findings suggest that the 21-nt 5′A-form of *TAS1c* 3′D10(−) may guide AGO2-mediated cleavage of *TAS1c* pri-RNA *in cis*. AGO2 is known to be associated with 21-nt 5′A-RNAs (15) but a slicer activity of AGO2 was not demonstrated so far.

In *ago2-1* mutant, apart from the reduced accumulation of 21-nt 3′D10(−), accumulation of other *TAS1c*-derived tasiRNAs including 3′D6(−) is not drastically affected (Figure 4A). This can be explained by increased (compensatory) production of tasiRNAs from *1c* dsRNA-D6 and also from *TAS1c* longest dsRNA. Indeed, accumulation of *1c* dsRNA-D6 is increased ∼2- to 3-fold in *ago2-1* compared to wild-type plants, concomitant with ∼2- to 3-fold decrease in accumulation of *1c*-dsRNA-D10; the longest dsRNA remains at a similar low level (Figure 5C and Supplementary Figure S4). Thus, in the absence of AGO2, *1c* dsRNA-D6 becomes the most abundant precursor of *TAS1c*-derived tasiRNAs.

Surprisingly, in *dcl2/3/4* plants that do not produce any tasiRNA, in addition to the longest *TAS1c* dsRNA, one shorter dsRNA accumulates to high levels (Figure 1). This dsRNA has 3′-overhangs of one to several nucleotides and is generated by a mechanism involving the miR173 cleavage and a precise cleavage that occurs predominantly 7-nt upstream of the 3′D6(−) cleavage site (Supplementary Figure S2C). It remains to be investigated which DCL1-dependent sRNA directs the second cleavage in this case.

The majority of *TAS1/TAS2* siRNAs are produced from the region between the cleavage sites

Our inspection of the deep-sequencing data (4) revealed that for each miR173-dependent *TAS* gene, most of unique sRNAs and the overwhelming majority of sRNA reads originate from the region between miR173 and *TAS1c* 3′D6(−) cleavage sites (Supplementary Figure S3B). Thus, the short dsRNAs (dsRNA-D6) produced by the two-cleavage mechanism are likely the major precursors of *TAS1/TAS2* tasiRNAs. The region of *TAS1a/b/c* and *TAS2* genes downstream of the *TAS1c* 3′D6(−) cleavage site also generates sRNAs, albeit at much lower levels (Supplementary Figure S3B). These sRNAs are likely processed from the longest, poly(A)/poly(U) duplex-containing dsRNAs.

TAS2- and *TAS1a/b/c*-derived short dsRNAs are processed from both ends

The dsRNAs derived from *TAS2*, *TAS1a*, *TAS1b* and *TAS1c* can potentially be processed from both ends. If this is true, then in addition to miR173-phased tasiRNAs, siRNAs in phase with the *TAS1c* 3′D6(−) cleavage site should also accumulate. Inspection of the deep-sequencing data (4) revealed that each of the four miR173-dependent *TAS* loci spawns 21-nt RNAs upstream of and in phase with the 3′D6(−) cleavage site (Supplementary Figure S3A; highlighted in pink). Also, more abundant 21-nt RNAs are produced in a 1-nt-forward-drifted phase caused by generation of 22-nt RNAs at the first (*TAS1a* and *TAS1b*) or the seventh processing cycle (*TAS2*) (Supplementary Figure S3A; purple). Thus, similar to miR390-directed cleavage for *TAS3* family pri-RNAs (12), the 3′D6(−) cleavage of *TAS1a/b/c* and *TAS2* pri-RNAs sets a register for production of phased siRNAs upstream of the cleavage site. This second register is shifted with respect of the miR173 register either forward (by 2 nt in *TAS2* and *TAS1c* and 3 nt in *TAS1a*) or backward (by 3 nt in *TAS1b*). Interestingly, an expected cleavage of *TAS1a* and *TAS2* pri-RNAs at the additional target sites for *TAS1c* 3′D6(−) (Figure 3) also appears to initiate processing of phased siRNAs from the upstream region (Supplementary Figure S3A; cyan and blue).

Likewise, *TAS1c* 3′D10(−) cleavage of *TAS1c* pri-RNA sets a register for 21-nt RNAs from the upstream region (Supplementary Figure S3A; green). Notably, the 22-nt *TAS1c* D10(−) species itself can be produced by in-phase processing of *1c* dsRNA-D6 from either end.

Using a miRNA target prediction software [http://bioinfo3.noble.org/psRNATarget/; (27)] we identified potential target genes for several siRNAs encoded in the registers set by the 3′D6(−) on *TAS1a*, *TAS1b* and *TAS2* and the 3′D10(−) on *TAS1c* (Supplementary Table S1).

Taken together, we conclude that the short dsRNAs derived from *TAS1a*, *TAS1b*, *TAS1c* and *TAS2* are processed by DCL4 not only from the miR173 end but also

from the opposite end defined by *TAS1c* 3′D6(−) cleavage and, in the case of *TAS1c,* also by *TAS1c* 3′D10(−) cleavage. The processing from both ends results in production of siRNAs in two different registers, thus increasing the coding capacity of these tasiRNA-generating loci.

It should be noted that the deep-sequencing data used for the above analyses of tasiRNAs were obtained using non-infected *A. thaliana* plants (4). Thus, the short dsRNA precursors of tasiRNAs identified here in CaMV-infected plants are likely present and processed from both ends in non-infected plants.

miR173-dependent tasiRNA production from *TAS1a/b* and *TAS2* genes is not drastically affected by *TAS1c* gene knockdown

Our results so far demonstrated that *TAS1c*-derived tasiRNA 3′D6(−) can target *in trans* *TAS1a/b* and *TAS2* pri-RNAs to initiate the biogenesis of abundant dsRNAs that can be processed by DCL4 from both ends. To address the question whether this second cleavage is required for efficient production of *TAS1a/b* and *TAS2* tasiRNAs in the miR173 register, we searched *A. thaliana* mutant collections for *TAS1c* gene mutants. By genotyping combined with RNA blot hybridization, we identified a homozygous mutant line (designated *tas1c-1*) with T-DNA insertion between the two major poly(A) sites of *TAS1c* (Supplementary Figure S2C). In *tas1c-1,* accumulation of *TAS1c* siRNAs including 3′D6(−) and 3′D10(−) was reduced to ∼40% of the wild-type level in rosette leaves and to ∼10% in inflorescence tissues (Figure 4A). This knockdown of *TAS1c* gene expression strongly reduced accumulation of the 3′D6(−)-dependent short dsRNAs derived from *TAS1a*, *TAS1b* and *TAS2* (Figure 4C; see 'dsRNA-D6' species highlighted in pink), but did not affect the accumulation the 3′D6(−)-independent, longest dsRNAs derived from *TAS1a* and *TAS1b* (Figure 4C; highlighted in blue) as well as less abundant, shorter RNAs derived from *TAS2* (Figure 4C; indicated by four connected arrows). The knockdown had only a slight impact on accumulation of *TAS1a/b* and *TAS2* tasiRNAs encoded in the miR173 register, which was reduced only to 70–80% of the wild-type levels in both tissues (Figure 4A). We conclude that *TAS1c* gene expression does not substantially affect the biogenesis of *TAS1a*, *TAS1b* and *TAS2*-derived siRNAs encoded in the miR173 register. Our findings are consistent with the notion that tasiRNA production from *TAS1a/b* and *TAS2* loci can proceed through a single miR173-directed cleavage event (18,19), which leads to the production of the longest, poly(A)/poly(U) duplex-containing dsRNAs.

TAS1c 3′D6(−) tasiRNA-directed cleavage regulates *TAS1c* 3′D10(−) siRNA biogenesis and precludes *TAS2* siRNA production downstream of the target site

To further investigate a role of the second cleavage of *TAS* pri-RNAs, we used a previously established transient expression assay using *N. benthamiana* leaves which recapitulates miR173-dependent tasiRNA biogenesis from the *TAS1 and TAS2* transcripts driven by the CaMV 35S promoter (10). Confirming the previous results, robust

production of siR255 from 35S:TAS1c and siR1940 from 35S:TAS2 could be achieved only by co-expression of miR173 from a 35S:miR173 construct. We then co-expressed the *TAS2* construct with 35S:TAS1c or its derivative in which the seed sequence of the 3′D6(−) tasiRNA had been mutated to prevent the second cleavage of *TAS2* pri-RNA. Co-expression of 3′D6(−) species or its seed-mutant form only slightly affected miR173-dependent production of siR1940 from *TAS2* (Figure 6), supporting the above conclusions. However, siRNA production from the region downstream of the 3′D6(−) cleavage site was nearly abolished in the presence of 3′D6(−) species but not its mutant form (see 'TAS2 D6 down' in Figure 6). Thus, the second cleavage of *TAS2* pri-RNA restricts siRNA production to the region between the miR173 and 3′D6(−) cleavage sites. This is consistent with our above analysis of the sRNA deep-sequencing data in *A. thaliana*. Interestingly, the region downstream of the 3′D6(−) cleavage site generated siRNAs of three size-classes and their production was detected both in the presence and absence of miR173.

For *TAS1c* itself, the mutation of the 3′D6(−) seed sequence did not alter miR173-dependent accumulation of siR255. However, it reduced accumulation of 22-nt 3′D10(−) and increased accumulation of 21-nt 3′D10(−) species, thus resembling the effect observed in *Arabidopsis ago1-25* plants. Mutation of the 3′D6(−) target site (TS) in 35S:TAS1c, in such a way that the mutant TS sequence could be cleaved only by the D6 seed-mutant siRNA but not the wild-type siRNA, led to a similar effect on accumulation of the 3′D10(−) size-classes. A combination of the two mutations restored the wild-type ratio of 3′D10(−) size-classes. Furthermore, an A-to-G mutation of the 5′-terminal nucleotide of the 21-nt 3′D10(−) in 35S:TAS1c increased the ratio of the 22-nt class to the 21-nt class, which is reminiscent of the effect observed in *Arabidopsis ago2-1* plants. Taken together, these results confirm feed-back regulation of *TAS1c* siRNA biogenesis by the 3′D6(−)-directed *in trans* cleavage and the 3′D10(−)-directed *in cis* cleavage of *TAS1c* pri-RNA.

DISCUSSION

Structures of RDR6-dependent dsRNA precursors of tasiRNAs

In this work we demonstrate that RDR6 converts the entire, polyadenylated, 3′-products of miR173-cleaved *TAS1/TAS2* pri-RNAs to dsRNA. However, the resulting longest dsRNAs accumulate at much lower levels than the shorter dsRNAs produced from all the four loci by a two-cleavage mechanism. In fact, *TAS2*-derived longest, poly(A)/poly(U) duplex-containing dsRNA could be detected only in *dcl2/3/4* plants lacking DCL2, DCL3 and DCL4 activities, while *TAS1 loci*-derived longest dsRNAs accumulated at much higher levels in *dcl2/3/4* than in wild-type plants. Thus, the polyadenylated 3′-fragment of miR173-cleaved *TAS* pri-RNAs is rapidly truncated by the second cleavage directed by *TAS1c*-derived tasiRNA 3′D6(−) which generates a shorter, poly(A)-less template for RDR6. We cannot exclude,
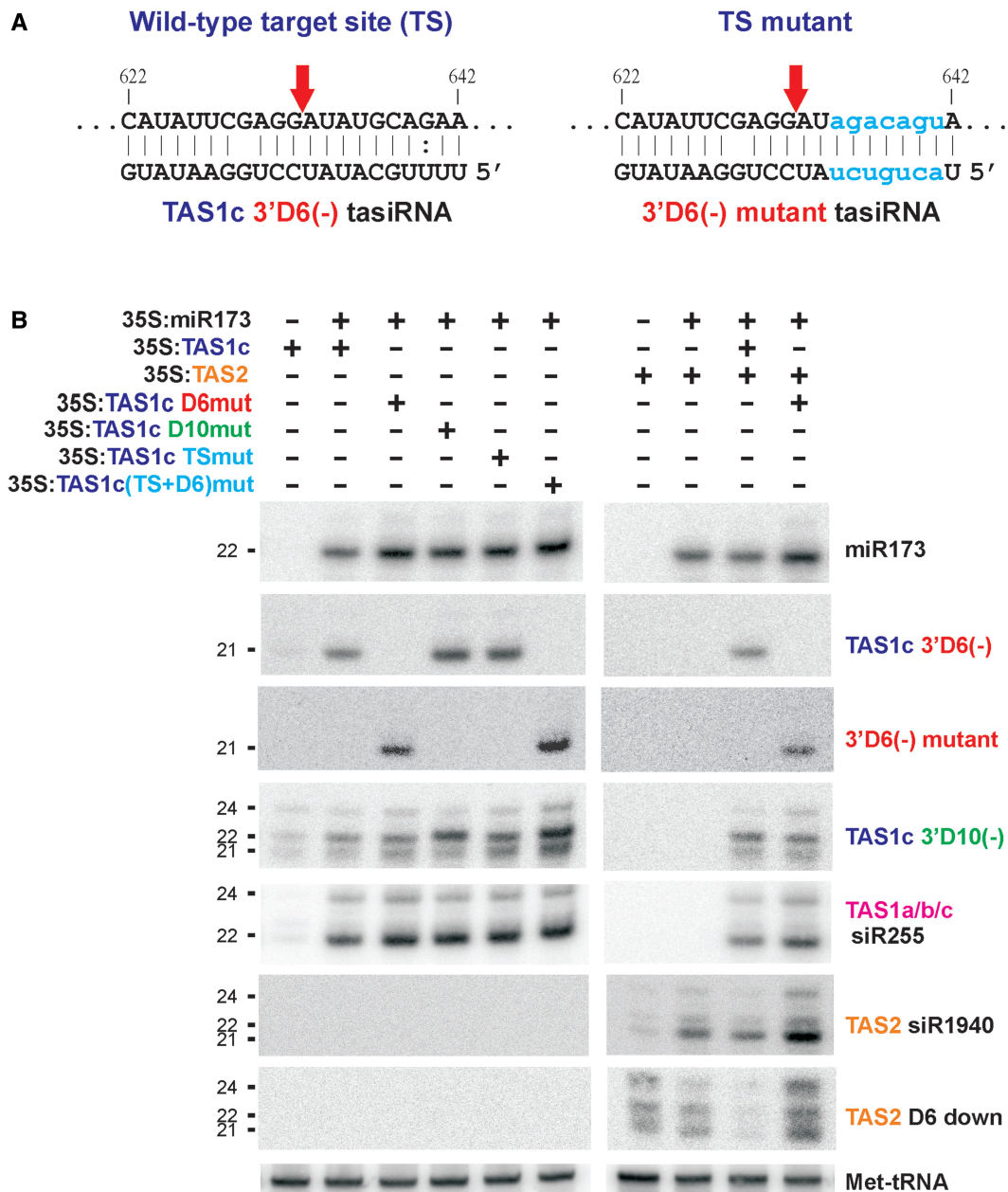
Figure 6. *TAS1c* 3′D6(−) tasiRNA-directed cleavage regulates *TAS1c* 3′D10(−) siRNA biogenesis and precludes *TAS2* siRNA production downstream of the target site. (**A**) The wild-type and mutant targets sites (TS) of the wild-type *TAS1c* pri-RNA and its TS mutant version, respectively. Mutagenized positions are in lower case and highlighted in cyan. Position of the cleavage directed by the wild-type *TAS1c* 3′D6(−) tasiRNA or its seed-mutant version is indicated by red arrow. (**B**) Reconstruction of *TAS1c* and *TAS2* tasiRNA biogenesis in a transient expression assay using *N. benthamiana*. 35S:TAS1c constructs with mutagenized 3′D6(−), 3′D10(−) siRNAs, the 3′D6(−) target site sequences, or both 3′D6(−) and its target site sequences were expressed or coexpressed with 35S:miR173 and also with 35S:TAS2 constructs as indicated above the blot panels. The siRNAs detected by successive hybridization of the blots are shown to the right of each panel.

however, that the longest dsRNA is more efficiently processed by DCL4 than the shorter dsRNA.

Our cRT-PCR analysis also suggests that the poly(A) tail is shortened and, in some cases, fully removed prior to RDR6 binding to the long template. The shortened poly(A) tails are often tagged by short UA-rich sequences. The RNA templates with both tagged and non-tagged poly(A) tails of up to 37 nt are copied by RDR6 to dsRNAs. This finding is supported by the *in vitro* studies

of an affinity-purified *A. thaliana* RDR6 protein showing that the RDR6 activity is not inhibited by addition of a 40-nt poly(A) tail to the template (28).

The structures of more abundant, short *TAS1/TAS2* dsRNAs identified here reveal that RDR6 initiates complementary RNA synthesis preferentially from the third nucleotide of the template's 3′-end, thus creating a 2-nt 3′-overhang on the resulting dsRNA. Less frequently, the synthesis is initiated from the second or the fourth

nucleotide, resulting in 1-nt or 3-nt 3′-overhangs, respectively. In our parallel work, precise mapping of the *TAS3a*-derived dsRNA revealed that RDR6 initiates complementary RNA synthesis predominantly at the third nucleotide of the miR390-cleaved *TAS3a* pri-RNA (17). This confirms our findings for miR173-dependent *TAS1/TAS2* dsRNAs. Furthermore, we demonstrate here that RDR6-mediated synthesis terminates at the 5′-terminal nucleotide of the template and frequently one or two non-template nucleotides are added to the 3′-end of the complementary RNA. Similar biochemical properties have been reported for an RDR activity isolated from tomato: this RDR copied an artificial single-stranded RNA template from the second or the third nucleotide of the template's 3′-terminus carrying the hydroxyl group and added one non-template nucleotide to 50% of the complementary run-off transcripts (25). Thus, production of dsRNAs with 1-nt or 2-nt 3′ overhangs at both termini appears to be a common property of plant RDRs. *In vitro* studies have shown that the dsRNA with a 2-nt 3′-overhang is an ideal substrate of human dicer (29). It remains to be investigated whether or not a short 3′ overhang is absolutely required for DCL4. Notably, a substantial fraction of miR173-dependent dsRNAs derived from *TAS1a*, *TAS1b*, *TAS1c* or *TAS2* does not possess any overhang at the miR173 cleavage end.

Our data also support the *in vitro* results showing that *Arabidopsis* RDR6 does not require a primer (28).

Role of the second cleavage of pri-RNA in tasiRNA production from *TAS1/TAS2* genes

We demonstrate here that miR173-initiated biogenesis of tasiRNAs from *Arabidopsis TAS2* and *TAS1* genes involves a second cleavage of *TAS* pri-RNA downstream of the miR173 site. In all cases, the short segment of pri-RNA between the two-cleavage sites is converted by RDR6 to dsRNA. The resulting dsRNA spans the region giving rise to the majority of siRNAs derived from each of the four loci. Hence, the two-cleavage mechanism generates the major dsRNA precursors of tasiRNAs. However, our results also demonstrate that the second cleavage is not required for production of tasiRNAs in the miR173 register. This is consistent with the previous studies showing that a single miR173-dependent cleavage is sufficient to initiate tasiRNA biogenesis (18,19). What could be the role of the second cleavage? Our results in *N. benthamiana* indicate that the second cleavage directed by *TAS1c* 3′D6(−) tasiRNA strongly reduces *TAS2* siRNA production from the region downstream of the cleavage site. Thus, the two-cleavage mechanism appears to restrict siRNA production to the region between the miR173 and 3′D6(−) cleavage sites. Additionally, identification of 21-nt phased siRNAs in the register set by *TAS1c* 3′D6(−) cleavage in the sRNA deep-sequencing database shows that the second cleavage could also be to increase the tasiRNA coding capacity of the *TAS1/TAS2* genes.

Our findings extend the two-hit trigger model originally proposed for miR390-dependent *TAS3* genes (12) to miR173-dependent *TAS1/TAS2* genes. But unlike *TAS3a/b/c* pri-RNAs targeted at two sites by a single miRNA (miR390), *TAS1a/b/c* and *TAS2* pri-RNAs are targeted by miR173 only at one site, while the second hit is guided by *TAS1c*-derived tasiRNA that cleaves not only *TAS1a*, *TAS1b* and *TAS2* pri-RNAs but also its own precursor (*TAS1c* pri-RNA). Previous studies have identified several *Arabidopsis* genes that have target sites for two or more different miRNAs and/or tasiRNAs; most of these genes generate secondary siRNAs (4,12). We demonstrate here that the miRNA- and the tasiRNA-directed cleavages at one target RNA can recruit RDR6 activity that converts the RNA segment between the two-cleavage sites to a dsRNA substrate for DCL4.

Feedback regulation of *TAS1c* gene

We propose a feedback regulation model in which *TAS1c* gene codes for two siRNAs, 3′D6(−) and 3′D10(−), which control tasiRNA production from this gene (Figure 4D). These siRNAs are encoded in antisense orientation at the processing cycles 6 and 10, in phase with the miR173 register, and can initially be generated from the poly(A)/poly(U) duplex-containing longest dsRNA, produced by RDR6 following a single miR173-cleavage. Once generated, each of these siRNAs together with miR173 directs cleavage of *TAS1c* pri-RNA at the respective target site to initiate RDR6-catalyzed synthesis of two distinct dsRNAs. The most abundant of the two (*1c* dsRNA-D10) is generated by the 3′D10(−) cleavage *in cis* and can potentially serve as a precursor of 3′D6(−) siRNA but not of 3′D10(−) itself. Less-abundant dsRNA (*1c* dsRNA-D6) generated by the 3′D6(−) cleavage *in trans* can potentially spawn both species (Figure 4D).

Several lines of evidence support our feedback model and allow speculation on potentially positive or negative functions of the two feedback loops. First, we have detected by blot hybridization and sequenced the three *TAS1c*-derived dsRNAs, namely, the single miR173-dependent longest dsRNA (*1c* dsRNA-long; Figures 1B and 2), the miR173- and *TAS1c* 3′D6(−) tasiRNA-dependent dsRNA (*1c* dsRNA-D6; Figures 1B and 3) and the miR173- and *TAS1c* 3′D10(−) siRNA-dependent dsRNA (*1c* dsRNA-D10; Figures 1B, 3 and 5). The terminal sequences of the dsRNA template strands indicate the conserved, AGO-mediated cleavages of *TAS1c* pri-RNA directed by miR173 on the upstream site and by the 3′D6(−) or 3′D10(−) siRNA at the downstream site. The relative accumulation levels of the three dsRNAs would suggest that DCL4 processing of the two shorter dsRNAs might generate the majority of *TAS1c*-derived siRNAs. However, we cannot exclude that the longest dsRNA is processed more efficiently than the shorter ones. Second, we provide genetic evidence that reduced accumulation of 21-nt 3′D10(−) siRNA in *ago2-1* mutant plants correlates with reduced accumulation of *1c* dsRNA-D10 and increased accumulation of *1c* dsRNA-D6 (Figure 5). Thus, the 3′D10(−)-directed cleavage required for *1c* dsRNA-D10 biogenesis appears to interfere with *1c* dsRNA-D6 biogenesis, possibly owing

to competition between 3′D10(−) and 3′D6(−) siRNAs for the same target *TAS1c* pri-RNA. This suggests that the *in cis* cleavage directed by 3′D10(−) may be involved in negative feedback regulation of *TAS1c* siRNA biogenesis. Third, our reconstitution of *TAS1c* siRNA production in the *N. benthamiana* transient assay shows that the 3′D6(−) tasiRNA-directed cleavage of *TAS1c* pri-RNA regulates the biogenesis of 3′D10(−) siRNA size-classes by decreasing relative accumulation of the cleavage-competent, 21-nt species (Figure 6), thus suggesting a positive function of this cleavage event. Further experiments are needed to clarify the roles of the two feedback loops in regulation of *TAS1c* gene expression.

We established that, similar to miR173, *TAS1c* 3′D6(−) tasiRNA is tightly associated with AGO1 protein to exert its function in *TAS1/TAS2* siRNA biogenesis. Interestingly, this 21-nt 5′U-RNA was also co-immunoprecipitated with AGO2 which preferentially binds 21-nt 5′A-RNAs and with AGO4 which preferentially binds 24-nt 5′A-RNAs [(15); Figure 5D]. We speculate that this apparent competition for the 3′D6(−) species may play a role in regulation of *TAS1c* expression by reducing the levels of functional AGO1::3′D6(−) complexes. Additionally, AGO4::3′D6(−) complex may function in the nucleus to downregulate transcription of *TAS1c* pri-RNA.

AGO2 was implicated in *TAS3* siRNA biogenesis and in antiviral defense since it was found to be associated with miR390 (15) and virus-derived siRNAs (16), respectively. Recently, the antiviral role of AGO2 was confirmed for some RNA viruses that encode suppressors specifically targeting AGO1 (30). However, so far there was no evidence for AGO2 catalytic activity. Our results suggest that this protein binds *TAS1c*-derived 21-nt siRNA 3′D10(−) to mediate *in cis* cleavage of *TAS1c* pri-RNA. Further experiments are needed to confirm that AGO2 is a functional slicer and that its slicer activity is required for AGO2 action in *TAS1c* tasiRNA biogenesis and antiviral defense.

TAS1/TAS2 gene regulation network

A sRNA interaction network connecting miR173-dependent *TAS2*, *TAS1a* and *TAS1c* genes was recently predicted by a bioinformatic analysis of sRNA populations sequenced from *A. thaliana* (6). Our data confirms the existence of this network as well as refines and extends the prediction by demonstrating that *TAS1c*-derived tasiRNA can target all the four miR173-dependent *TAS* loci. Few unmapped RNAs that we detected by blot hybridization (Figure 1) may arise from additional targeting events predicted by MacLean *et al.* (6).

The existence of this complex network with a central role for *TAS1c* is not surprising, given the fact that the four *TAS* loci are paralogous: *TAS2* and *TAS1c* arose by a direct duplication, while *TAS1a* and *TAS1b* arose from *TAS1c* after it had diverged from *TAS2* (11). Interestingly, *TAS2* and *TAS1* tasiRNAs including *TAS1c* 3′D6(−) and 3′D10(−) described here target several pentatricopeptide repeat family genes giving rise to secondary siRNAs with the potential to target *in trans* other genes within and outside of this multigene family (4). This creates another complex interaction network subordinate to the miR173 network. Our findings for *TAS1c* would also suggest that feedback loops in the hubs of sRNA networks can fine-tune the levels of a master siRNA, such as *TAS1c* 3′D6(−), required for *in trans* regulation of other genes.

SUPPLEMENTARY DATA

Supplementary Data are available at NAR Online: Supplementary Figures 1, 2 (A, B, C and D), 3 (A and B) and 4, Supplementary Table 1, Supplementary Methods and Inventory of Supplementary Data.

REFERENCES

1. Chapman,E.J. and Carrington,J.C. (2007) Specialization and evolution of endogenous small RNA pathways. *Nat. Rev. Genet.*, **8**, 884–896.
2. Voinnet,O. (2009) Origin, biogenesis, and activity of plant microRNAs. *Cell*, **136**, 669–687.
3. Rajagopalan,R., Vaucheret,H., Trejo,J. and Bartel,D.P. (2006) A diverse and evolutionarily fluid set of microRNAs in Arabidopsis thaliana. *Genes Dev.*, **20**, 3407–3425.
4. Howell,M.D., Fahlgren,N., Chapman,E.J., Cumbie,J.S., Sullivan,C.M., Givan,S.A., Kasschau,K.D. and Carrington,J.C. (2007) Genome-wide analysis of the RNA-DEPENDENT RNA POLYMERASE6/DICER-LIKE4 pathway in Arabidopsis reveals dependency on miRNA- and tasiRNA-directed targeting. *Plant Cell*, **19**, 926–942.
5. Chen,H.M., Chen,L.T., Patel,K., Li,Y.H., Baulcombe,D.C. and Wu,S.H. (2010) 22-Nucleotide RNAs trigger secondary siRNA biogenesis in plants. *Proc. Natl Acad. Sci. USA*, **107**, 15269–15274.
6. MacLean,D., Elina,N., Havecker,E.R., Heimstaedt,S.B., Studholme,D.J. and Baulcombe,D.C. (2010) Evidence for large complex networks of plant short silencing RNAs. *PLoS One*, **5**, e9901.
7. Chen,X. (2009) Small RNAs and their roles in plant development. *Annu. Rev. Cell Dev. Biol.*, **25**, 21–44.
8. Ruiz-Ferrer,V. and Voinnet,O. (2009) Roles of plant small RNAs in biotic stress responses. *Annu. Rev. Plant Biol.*, **60**, 485–510.

9. Katiyar-Agarwal,S. and Jin,H. (2010) Role of small RNAs in host-microbe interactions. *Annu. Rev. Phytopathol.*, **48**, 225–246.

10. Allen,E., Xie,Z., Gustafson,A.M. and Carrington,J.C. (2005) microRNA-directed phasing during trans-acting siRNA biogenesis in plants. *Cell*, **121**, 207–221.

11. Yoshikawa,M., Peragine,A., Park,M.Y. and Poethig,R.S. (2005) A pathway for the biogenesis of trans-acting siRNAs in Arabidopsis. *Genes Dev.*, **19**, 2164–2175.

12. Axtell,M.J., Jan,C., Rajagopalan,R. and Bartel,D.P. (2006) A two-hit trigger for siRNA biogenesis in plants. *Cell*, **127**, 565–577.

13. Montgomery,T.A., Howell,M.D., Cuperus,J.T., Li,D., Hansen,J.E., Alexander,A.L., Chapman,E.J., Fahlgren,N., Allen,E. and Carrington,J.C. (2008) Specificity of ARGONAUTE7-miR390 interaction and dual functionality in TAS3 trans-acting siRNA formation. *Cell*, **133**, 128–141.

14. Montgomery,T.A., Yoo,S.J., Fahlgren,N., Gilbert,S.D., Howell,M.D., Sullivan,C.M., Alexander,A., Nguyen,G., Allen,E., Ahn,J.H. *et al.* (2008) AGO1-miR173 complex initiates phased siRNA formation in plants. *Proc. Natl Acad. Sci. USA*, **105**, 20055–20062.

15. Mi,S., Cai,T., Hu,Y., Chen,Y., Hodges,E., Ni,F., Wu,L., Li,S., Zhou,H., Long,C. *et al.* (2008) Sorting of small RNAs into Arabidopsis argonaute complexes is directed by the 5′ terminal nucleotide. *Cell*, **133**, 116–127.

16. Takeda,A., Iwasaki,S., Watanabe,T., Utsumi,M. and Watanabe,Y. (2008) The mechanism selecting the guide strand from small RNA duplexes is different among argonaute proteins. *Plant Cell Physiol.*, **49**, 493–500.

17. Rajeswaran,R. and Pooggin,M.M. (2012) RDR6-mediated synthesis of complementary RNA is terminated by miRNA stably bound to template RNA. *Nucleic Acids Res.*, **40**, 594–599.

18. Cuperus,J.T., Carbonell,A., Fahlgren,N., Garcia-Ruiz,H., Burke,R.T., Takeda,A., Sullivan,C.M., Gilbert,S.D., Montgomery,T.A. and Carrington,J.C. (2010) Unique functionality of 22-nt miRNAs in triggering RDR6-dependent siRNA biogenesis from target transcripts in Arabidopsis. *Nat. Struct. Mol. Biol.*, **17**, 997–1003.

19. Chen,H.M., Li,Y.H. and Wu,S.H. (2007) Bioinformatic prediction and experimental validation of a microRNA-directed tandem trans-acting siRNA cascade in Arabidopsis. *Proc. Natl Acad. Sci. USA*, **104**, 3318–3323.

20. Manavella,P.A., Koenig,D. and Weigel,D. (2012) Plant secondary siRNA production determined by microRNA-duplex structure. *Proc. Natl Acad. Sci. USA.*, **109**, 2461–2466.

21. Shivaprasad,P.V., Rajeswaran,R., Blevins,T., Schoelz,J., Meins,F. Jr, Hohn,T. and Pooggin,M.M. (2008) The CaMV transactivator/viroplasmin interferes with RDR6-dependent trans-acting and secondary siRNA pathways in Arabidopsis. *Nucleic Acids Res.*, **36**, 5896–5909.

22. Blevins,T., Rajeswaran,R., Shivaprasad,P.V., Beknazariants,D., Si-Ammour,A., Park,H.S., Vazquez,F., Robertson,D., Meins,F. Jr, Hohn,T. *et al.* (2006) Four plant Dicers mediate viral small RNA biogenesis and DNA virus induced silencing. *Nucleic Acids Res.*, **34**, 6233–6246.

23. Shivaprasad,P.V., Akbergenov,R., Trinks,D., Rajeswaran,R., Veluthambi,K., Hohn,T. and Pooggin,M.M. (2005) Promoters, transcripts, and regulatory proteins of Mungbean yellow mosaic geminivirus. *J. Virol.*, **79**, 8149–8163.

24. Blevins,T., Rajeswaran,R., Aregger,M., Borah,B.K., Schepetilnikov,M., Baerlocher,L., Farinelli,L., Meins,F., Hohn,T. and Pooggin,M.M. (2011) Massive production of small RNAs from a non-coding region of Cauliflower mosaic virus in plant defense and viral counter-defense. *Nucleic Acids Res.*, **39**, 5003–5014.

25. Schiebel,W., Haas,B., Marinković,S., Klanner,A. and Sänger,H.L. (1993) RNA-directed RNA polymerase from tomato leaves. II. Catalytic in vitro properties. *J. Biol. Chem.*, **268**, 11858–11867.

26. Morel,J.B., Godon,C., Mourrain,P., Béclin,C., Boutet,S., Feuerbach,F., Proux,F. and Vaucheret,H. (2002) Fertile hypomorphic ARGONAUTE (ago1) mutants impaired in post-transcriptional gene silencing and virus resistance. *Plant Cell*, **14**, 629–639.

27. Dai,X., Zhuang,Z. and Zhao,P.X. (2010) Computational analysis of miRNA targets in plants: current status and challenges. *Brief Bioinform.*, **12**, 115–121.

28. Curaba,J. and Chen,X. (2008) Biochemical activities of Arabidopsis RNA-dependent RNA polymerase 6. *J. Biol. Chem.*, **283**, 3059–3066.

29. Zhang,H., Kolb,F.A., Jaskiewicz,L., Westhof,E. and Filipowicz,W. (2004) Single processing center models for human Dicer and bacterial RNase III. *Cell*, **118**, 57–68.

30. Harvey,J.J., Lewsey,M.G., Patel,K., Westwood,J., Heimstädt,S., Carr,J.P. and Baulcombe,D.C. (2011) An antiviral defense role of AGO2 in plants. *PLoS One*, **6**, e14639.